https://doi.org/10.5194/egusphere-2025-969
Preprint. Discussion started: 14 April 2025
© Author(s) 2025. CC BY 4.0 License.

Machine learning-based Alpine treeline detection in Xue Mountain of Taiwan

Geng-Gui Wang[1], Min-Chun Liao[2], Wei Wang[3], Hui Ping Tsai[1,4,*], Hsy-Yu Tzeng[5]

[1]Department of Civil Engineering, and Innovation and Development Center of Sustainable Agriculture, National Chung Hsing University, Taichung City 402, Taiwan (R.O.C.)
[2] Chiayi Research Center, Taiwan Forestry Research Institute, Chiayi City 600, Taiwan (R.O.C.)
[3] Experimental Forest, National Chung Hsing University, No. 145 Xingda Rd., Taichung City 402, Taiwan (R.O.C.)
[4] i-Center for Advanced Science and Technology, National Chung Hsing University, Taichung City 402, Taiwan (R.O.C.)
[5] Department of Forestry, National Chung Hsing University, Taichung City 402, Taiwan (R.O.C.)

Correspondence to: Hui-Ping Tsai (email)

Abstract. Taiwan has the highest density of high mountains globally, with over 200 peaks exceeding 3,000 meters in elevation. The Alpine Treeline Ecotone (ATE) is a transitional zone between different vegetation types. The species distribution, range variations, and movement patterns of vegetation within the ATE are crucial indicators for assessing the impact of climate change and warming on alpine ecosystems. Therefore, this study focuses on the Xue Mountain glacial cirques in Taiwan (approximately 4 km²) and utilizes WorldView-2 satellite images from 2012 and 2021 to compute various vegetation indices and texture features (GLCM). By integrating these features with the Random Forest (RF) and U-Net models, we developed a classification map of the alpine treeline ecotone (ATE) in Xue Mountain. We analyzed changes in bare land, forest, krummholz, and shadows within the ATE from 2012 to 2021. The results indicate that the classification accuracy reached an overall accuracy (OA) of 0.838 when incorporating raw spectral bands along with vegetation indices and texture features (GLCM) (77 features in total). Feature importance ranking and selection reduced training time by 14.3% while ensuring alignment between field survey treeline positions and classification results. From 2012 to 2021, tree cover density increased, with the total forest area expanding by approximately 0.101 km². The elevation of tree distribution rose by 14 m, with the most significant area changes occurring between 3,500 and 3,600 m, while the 3,700 to 3,800 m range remained relatively stable. This study integrates remote sensing imagery with deep learning classification methods to establish a large-scale alpine treeline ecotone (ATE) classification map. The findings provide a valuable reference for the sustainable management of alpine ecosystems in the Xue Mountain glacial cirques in Taiwan.

https://doi.org/10.5194/egusphere-2025-969
Preprint. Discussion started: 14 April 2025
© Author(s) 2025. CC BY 4.0 License.

1 Introduction

Taiwan is located in the subtropical region of Southeast Asia, with an elevation range of nearly 4,000 m, fostering diverse ecosystem types and rich biodiversity (Lin et al., 2021). The island contains more than 200 mountains exceeding 3,000 meters in elevation (Kuo et al., 2022), making it the highest-density alpine island in the world. Alpine zone ecosystems are susceptible to environmental changes compared to other regions (Engler et al., 2011; Huss et al., 2017; Li et al., 2018; Zheng et al., 2020). The transition zone between trees and treeless vegetation in alpine ecosystems is known as the alpine treeline or the Alpine Treeline Ecotone (ATE) (Körner 2012). The ecological processes and changes in this zone are considered indicators of climate change (Chen et al., 2022), reflecting the interactions of climate, topography, species composition, and disturbance history (Loranger et al., 2016; Johnson et al., 2017; Mohapatra et al., 2019; Bader et al., 2020). Furthermore, ATE changes illustrate the impact of climate change on the environment, such as the upward migration of tree species and an increase in tree density (Wang et al., 2016; Johnson et al., 2017; Du et al., 2018; Mohapatra et al., 2019).

In recent years, with the advancement of remote sensing technology, many scholars have employed remote sensing imagery to study alpine treelines. Xu et al. (2020) utilized Landsat satellite imagery from 1987 to 2018 for Wuyishan National Park, China. They examined the relationship between treeline position and climate based on the local indicator of spatial autocorrelation (LISA). Their study found that from 1987 to 2018, for every 1°C increase in temperature, the treeline shifted upward by 50 m. Rösch et al. (2022) used 2020 PlanetScope and Sentinel-2 satellite imagery, incorporating texture features from the gray level co-occurrence matrix (GLCM), topographic features, and the canopy height model (CHM) to map the distribution of mountain pine (*Pinus mugo ssp. Mugo Turra*) in the Sarntal Alps. Their results indicated that combining satellite images with all features could accurately map the distribution of mountain pine forests, with an accuracy of 90.96% for PlanetScope imagery and 90.65% for Sentinel-2 imagery. Terskaia et al. (2020) analyzed the invasion of trees and tall shrubs into the tundra in the western Brooks Range, Alaska, using orthophoto aerial images from 1952 and 1979, along with WorldView-2 satellite imagery from 2015. Their study found that between 1952 and 2015, arctic and alpine tundra areas decreased by 31% and 15%, respectively, while tall shrubs, mixed tree-shrub areas, and forests increased by 86%, 385%, and 84%, respectively. The average treeline was located at an elevation of 202 meters. These studies collectively confirm the reliability of remote sensing technology in researching alpine treeline changes.

The integration of machine learning with remote sensing has also been successfully applied to forest studies, with many scholars reporting favorable results using the Random Forest (RF) and U-Net models. Jombo et al. (2020) used WorldView-2 imagery with RF and Support Vector Machines (SVM) models to classify five types of street trees in the complex urban environment of Randburg municipal, achieving overall accuracies of 84.2% and 81.2%, respectively. Similarly, Jackson and Adam (2021) employed WorldView-2 imagery with RF and SVM to classify endangered tree species in the Mount Kenya Forest Reserve (MKFR), finding that RF outperformed SVM. Wagner et al. (2019) applied a U-Net convolutional network to identify forests in the Atlantic rainforest region of Brazil using ultra-high-resolution WorldView-3 satellite imagery. They classified artificial forests, natural forests, and the *Cecropia hololeuca*, achieving an overall segmentation accuracy of over

https://doi.org/10.5194/egusphere-2025-969
Preprint. Discussion started: 14 April 2025
© Author(s) 2025. CC BY 4.0 License.

95%, with an Intersection-over-Union (IoU) of 0.96. The classification accuracy for *Cecropia hololeuca* species reached 97%, with an IoU of 0.86. Freudenberg et al. (2019) used WorldView-2 and WorldView-3 imagery in Indonesia to detect Oil and coconut palm tree distribution. In addition to evaluating U-Net's detection accuracy, they assessed its processing speed, finding that the U-Net-based model achieved a maximum throughput of 235 hectares per second at a 40 cm resolution. The model demonstrated high generalizability, with detection accuracies ranging from 89% to 92% across different regions. Their study suggested that this method could be used for rapid nationwide detection of oil palm distribution. Based on these studies, applying high-resolution WorldView satellite imagery combined with RF and U-Net machine learning models offers accuracy, cost efficiency, and generalizability advantages for ecological remote sensing classification. Therefore, this study will integrate WorldView-2 satellite imagery with RF and U-Net models to classify alpine treelines, find important features, and understand the change and spatial patterns in the Xue Mountain glacial cirques region in Taiwan.

2 Materials and methods

2.1 Study site

The Xue Mountain glacial cirques are located in Shei-Pa National Park in north-central Taiwan, covering an area of approximately 4 km². The central peak of Xueshan has an elevation of 3,886 m. The cirque serves as a crucial habitat for Taiwan's endemic species, the Yushan Juniper (*Juniperus morrisonicola*), Yushan rhododendron (*Rhododendron pseudochrystam*), and the Taiwan fir (*Abies kawakamii*), which is primarily distributed at elevations between 3,000 and 3,600 m. Several researchers have been conducting studies on the volume estimation, competitive pressure, forest structure, and spatial distribution of the Taiwan fir, primarily through field surveys (Li et al., 2021; Wang et al., 2021; Chiu et al., 2022; Liao et al., 2023a; Liao et al., 2023b). The study area is shown in Fig. 1.

https://doi.org/10.5194/egusphere-2025-969
Preprint. Discussion started: 14 April 2025
© Author(s) 2025. CC BY 4.0 License.

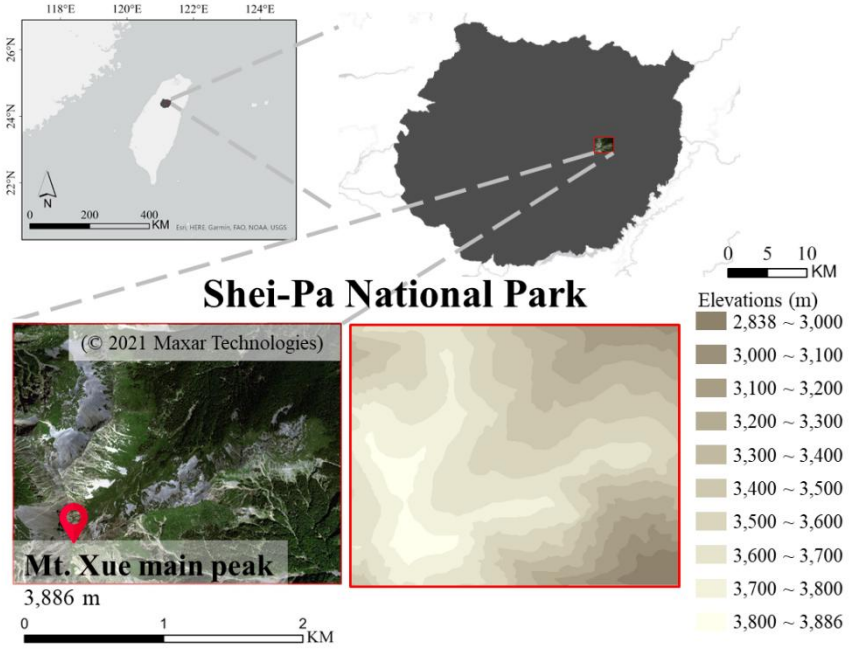

Figure 1: study site

2.2 Research flow

This study utilizes WorldView-2 satellite imagery from 2021 to extract raw spectral bands, vegetation indices, and texture features. Starting with the eight spectral bands, vegetation indices, and texture features are sequentially added to form four different feature combinations. Classification models are developed using the RF and U-Net models, and the optimal model is selected. This model is then applied to 2012 imagery to map the distribution of the alpine treeline and analyze changes over the decade. The research workflow is illustrated in Fig. 2.

https://doi.org/10.5194/egusphere-2025-969
Preprint. Discussion started: 14 April 2025
© Author(s) 2025. CC BY 4.0 License.

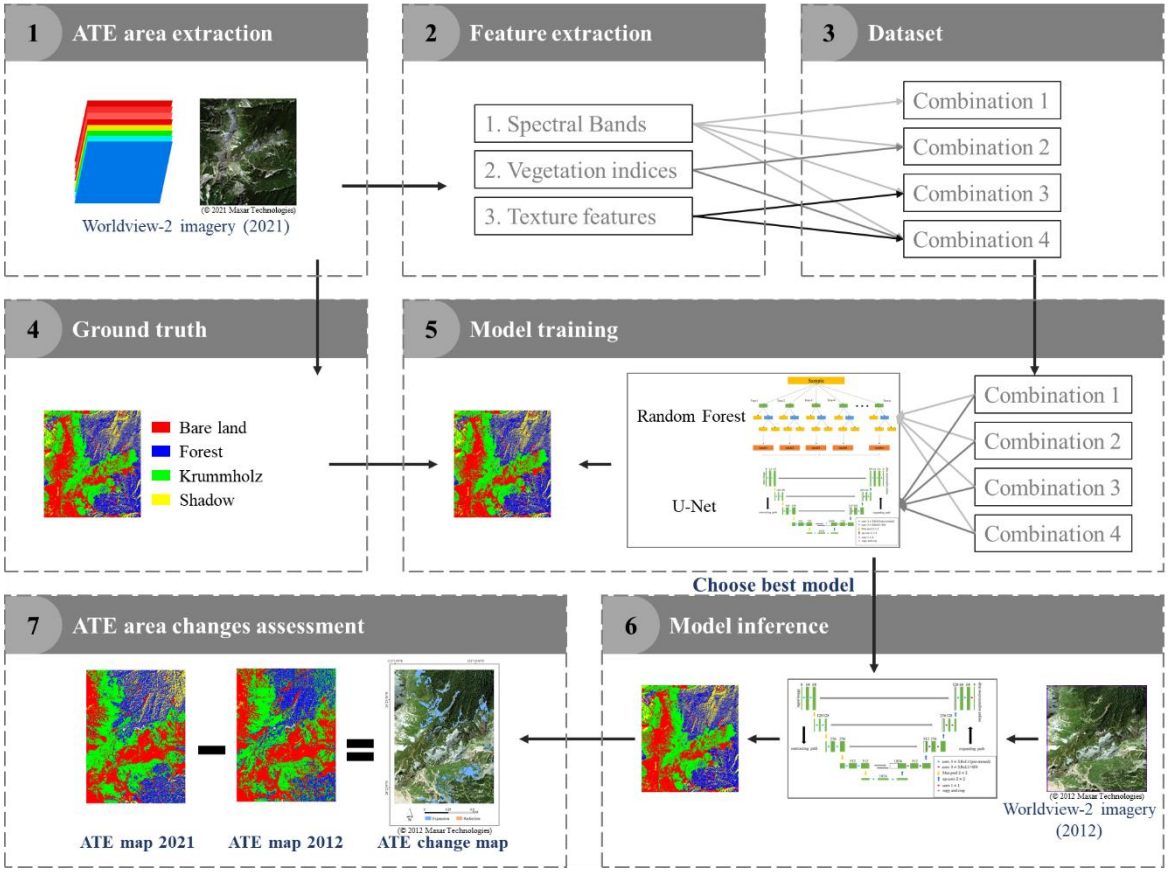

Figure 2: Research flow

2.3 Research data

The research data sources are categorized into satellite imagery and field surveys, with satellite imagery as the primary source and field surveys used as supplementary validation to ensure the accuracy of the treeline boundary. WorldView-2 is an environmental monitoring satellite operated by Maxar Technologies Inc. (Colorado, USA). It was launched on October 8, 2009, and its geolocation accuracy, even without any ground control points, is within 3 meters. Depending on the spatial resolution, the revisit time ranges from 1.1 to 3.7 days. The satellite provides two imaging modes: panchromatic and multispectral. The spatial resolution is 0.41 m in the panchromatic mode, and the spectral range spans 450–800 nm. This mode offers high spatial resolution, allowing for detailed image representation. In the multispectral mode, the spatial resolution is 1.64 m, and the spectral range extends from 400 to 1040 nm, covering eight spectral bands, as shown in Table 1. For this study, two cloud-free WorldView-2 orthorectified images with a spatial resolution of 0.4 meters, acquired on November 3, 2012, and September 26, 2021, were obtained through RiChi Technology Co., Ltd. (New Taipei City, Taiwan), and GPS was used to record survey points.

https://doi.org/10.5194/egusphere-2025-969
Preprint. Discussion started: 14 April 2025
© Author(s) 2025. CC BY 4.0 License.

Table 1: Worldview-2 Satellite image band introduction

Band	Spectral range (nm)	Data quantization (Bits)
Costal Blue (CB)	400-450	11
Blue (B)	450-510	
Green (G)	510-580	
Yellow (Y)	585-625	
Red (R)	630-690	
Red Edge (RE)	703-745	
Near Infrared 1 (NIR1)	770-895	
Near Infrared 2 (NIR2)	860-1040	

2.4 Vegetation Index

The reflectance spectrum of plant leaves can reflect their internal physiological status, such as chlorophyll content, water content, intercellular spaces, and cell walls. The frequently discussed spectral bands include red (R), the red edge (RE), and the near-infrared (NIR) bands. Derived vegetation indices, such as the Normalized Difference Vegetation Index (NDVI) and the Enhanced Vegetation Index (EVI), have been widely used (Rouse et al., 1974; Huete et al., 2002). Additionally, some studies have suggested that the blue (B) and green (G) bands can be used to monitor vegetation phenology and forests. For example, indices such as the Green Chromatic Coordinate (GCC) and the Excess Green Index (ExG) have been developed for this purpose (Sonnentag et al., 2012; Larrinaga and Brotons, 2019). Since image acquisition is affected by terrain, leading to shadow occurrences that influence classification accuracy, this study also plans to adopt the Shadow-Eliminated Vegetation Index (SEVI) (Jiang et al., 2019). This study will utilize 11 vegetation indices, as summarized in Table 2.

Table 2: Vegetation indices and their formulas

Vegetation Index	Formula	Reference
Difference Vegetation Index (DVI)	$\mathrm{NIR} - \mathrm{R}$	Richardson and Wiegand, 1977
Enhanced vegetation index (EVI)	$2.5 \times \frac{(\mathrm{NIR} - \mathrm{R})}{(\mathrm{NIR} + 6 \times \mathrm{R} - 7.5 \times \mathrm{B} + 1)}$	Huete et al., 2002
Excess Blue Vegetation Index (ExB)	$\frac{1.4 \times \mathrm{B} - \mathrm{G}}{\mathrm{G} + \mathrm{R} + \mathrm{B}}$	Mao et al., 2003
Excess Green Index (ExG)	$\frac{2 \times \mathrm{G} - \mathrm{R} - \mathrm{B}}{\mathrm{G} + \mathrm{R} + \mathrm{B}}$	Woebbecke et al., 1995
Excess Green minus Excess Red (ExGR)	$\mathrm{ExG} - \mathrm{ExR}$	Meyer and Neto, 2008

https://doi.org/10.5194/egusphere-2025-969
Preprint. Discussion started: 14 April 2025
© Author(s) 2025. CC BY 4.0 License.

Excess Red Vegetation Index (ExR)	$\frac{1.4 \times \mathrm{R} - \mathrm{G}}{\mathrm{G} + \mathrm{R} + \mathrm{B}}$	Meyer et al., 1999
The Green Chromatic Coordinate (GCC)	$\mathrm{G}/(\mathrm{R} + \mathrm{G} + \mathrm{B})$	Gillespie et al., 1987
Normalized difference index (NDI)	$\frac{\mathrm{G} - \mathrm{R}}{\mathrm{G} + \mathrm{R}}$	Gitelson and Merzlyak, 1994
Normalized difference vegetation index (NDVI)	$\frac{\mathrm{NIR} - \mathrm{R}}{\mathrm{NIR} + \mathrm{R}}$	Rouse et al., 1974
Ratio Vegetation Index (RVI)	$\frac{\mathrm{NIR}}{\mathrm{R}}$	Jordan, 1969
Shadow- Eliminated Vegetation Index (SEVI)	$\mathrm{RVI} + f(\Delta) \times \frac{1}{\mathrm{R}}$	Jiang et al., 2019

2.5 Texture Feature

With the improvement in the spatial resolution of satellite imagery, most ground objects are composed of multiple pixels, making the spatial attributes of images increasingly important (Wang et al., 2015). Texture features extract the structural and arrangement properties of ground objects, which describe the spatial attributes of objects in an image. As one of the key features for image interpretation, texture helps distinguish land cover types with similar spectral characteristics. Texture analysis methods can be categorized into spectral, statistical, and structural approaches, with the Gray Level Co-occurrence Matrix (GLCM) in statistical approaches being the most commonly used (Hsu, 1978). Guo et al. (2020) applied texture features to map the forest-tundra ecotone in central Eurasia. They found that texture-based classification maps performed better than previous methods, achieving an average classification accuracy of 0.826. Similarly, Sibiya et al. (2021) used WorldView-2 satellite imagery to classify forest species in South Africa. They found that texture features improved overall classification accuracy by approximately 8% compared to vegetation indices and 13% compared to original spectral bands. Their study also observed that a moving window size of 7 × 7 produced the best results. Therefore, this study adopted a 7 × 7 moving window to compute the GLCM matrix for each of the eight bands, analysing seven statistical metrics, resulting in 56 texture features. The seven statistical metrics used in this study are listed in Table 3.

Table 3: Texture Feature and their formulas

Texture Feature	Formula	Reference
Contrast (Con)	$\sum_{i,j=0}^{N-1} P_{i,j}(i-j)^2$	Yuan et al., 1991
Dissimilarity (Dis)	$\sum_{i,j=0}^{N-1} P_{i,j}\lvert i-j\rvert$	Rubner et al., 2002

https://doi.org/10.5194/egusphere-2025-969
Preprint. Discussion started: 14 April 2025
© Author(s) 2025. CC BY 4.0 License.

Energy (Ene)	$\sum_{i,j=0}^{N-1} {P_{i,j}}^2$	Hall-Beyer, 2017
Entropy (Ent)	$\sum_{i,j=0}^{N-1} P_{i,j}(-lnP_{i,j})$	Yuan et al., 1991
Homogeneity (Hom)	$\sum_{i,j=0}^{N-1} \frac{P_{i,j}}{1+(i-j)^2}$	Hall-Beyer, 2017
Mean (M)	$\sum_{i,j=0}^{N-1} iP_{i,j}$	Materka and Strzelecki, 1998
Variance (Var)	$\sum_{i,j=0}^{N-1} P_{i,j}(i-\text{Mean})^2$	Materka and Strzelecki, 1998

$P_{i,j}$ is the gray-level co-occurrence matrix after normalization.

2.6 Methods

2.6.1 Random Forest (RF)

Random Forests (RF) is an ensemble classifier widely used in remote sensing due to its ability to handle high-dimensional data. It generates multiple decision trees (DTs), where each tree makes predictions based on observed features through a series of decision-making steps, ultimately concluding the target variable. Decision trees, also known as classification trees, are a type of predictive model. Random forests use the Bagging algorithm (Bootstrap Aggregating) as their core classification mechanism. The process begins by randomly sampling the data to create training datasets. After each sampling, the selected data points are returned to the dataset for the next round of sampling (bootstrap sampling). This process is repeated multiple times, resulting in several training datasets, which are then used to train multiple decision trees. This approach allows for scenarios where specific data points are sampled multiple times while others may not. Each decision tree selects a random subset of features at each node to determine the best split, ultimately generating predictions from each tree. The final classification result is determined by aggregating all decision tree predictions using a majority voting approach. The model also utilizes the Gini Index, calculated using the following formula: the Gini Index represents the out-of-bag (OOB) error rate. This metric is used to assess the contribution of each feature to the model, serving as an indicator of feature importance (Belgiu and Drăguţ, 2016; Breiman, 2001; Chen et al., 2023).

$$Gini_m = \sum_{k=1}^{k} \hat{p}_{mk}(1-\hat{p}_{mk}) , \quad (1)$$

Where K represents the number of classes in the training samples, and $\hat{p}_{mk}$ denotes the probability of sample m belonging to class k.

https://doi.org/10.5194/egusphere-2025-969
Preprint. Discussion started: 14 April 2025
© Author(s) 2025. CC BY 4.0 License.

155

2.6.2 U-Net

Ronneberger et al. (2015) proposed the original U-Net model, which evolved from the fully connected network (FCN) and was initially applied to biomedical image segmentation. The model is named U-Net because its architecture resembles a U-shaped structure. It is also a shallow convolutional neural network (CNN) segmentation model. The U-Net model consists of a contracting path (downsampling) and an expanding path (upsampling). Similar to FCN, U-Net does not have fully connected layers, and its use of convolutional layers significantly reduces the amount of training data required while allowing inputs of different sizes. Before entering the contracting or expanding path, the data undergoes two consecutive convolutional layers, which help the network extract target features more effectively. This process also enhances the integration of fine details with feature maps, thereby improving segmentation quality. Each convolutional layer is followed by a rectified linear unit (ReLU) activation function, which enhances training efficiency without affecting model accuracy. The pooling layer at the bottom serves as a nonlinear form of downsampling, reducing the spatial size of the data, decreasing the number of parameters and computational costs, and helping to control overfitting. Since U-Net lacks fully connected layers, it effectively minimizes information loss caused by downsampling and preserves finer image details.

2.6.3 Data set

The WorldView-2 satellite imagery consists of eight spectral bands (CB, B, G, Y, R, RE, NIR1, NIR2). Based on these eight bands, this study derived 13 vegetation indices and 56 texture features, resulting in 77 feature variables. The original eight bands were incrementally combined with vegetation indices and texture features, forming four different feature combinations, as shown in Table 4. Ground truth data in the study area were labeled using a pixel-based approach and categorized into four classes: bare land, forest, krummholz, and shadow (Fig. 3). Each image (5380 × 4671 pixels) was segmented into smaller images of 512 × 512 pixels, yielding a total of 110 images. The dataset was randomly split, with 80% used for training and validation and 75% and 25% allocated for training and validation, respectively. The remaining 20% was designated as the test dataset. The number of images used for training, validation, and testing was 66, 22, and 22, respectively.

Table 4: Combination of features designed in this study

Feature combinations	Input feature	Feature Dimension
1	spectral band	8
2	spectral band, vegetation indices	21
3	spectral band, texture features	64
4	spectral band, vegetation indices, texture features	77

https://doi.org/10.5194/egusphere-2025-969
Preprint. Discussion started: 14 April 2025
© Author(s) 2025. CC BY 4.0 License.

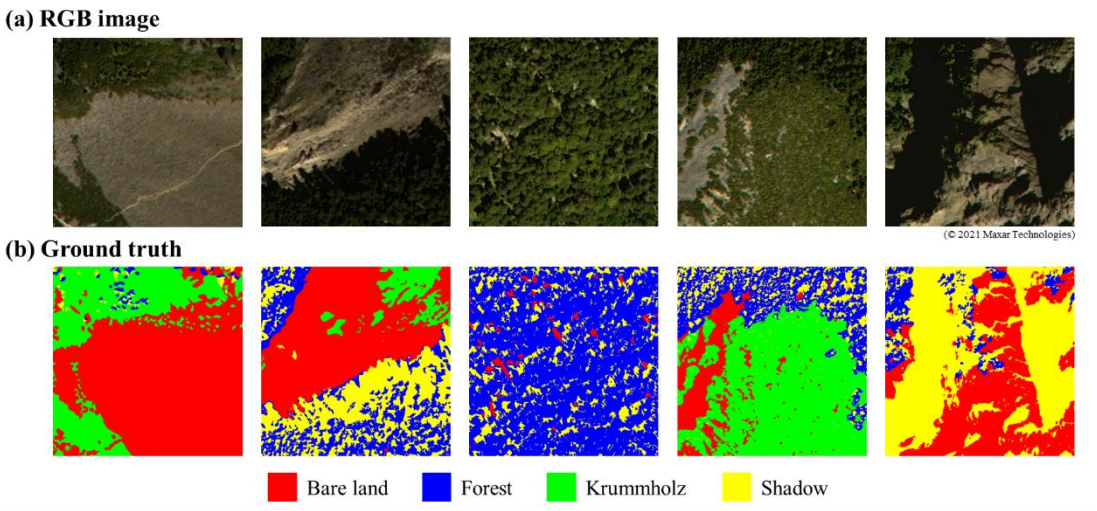

Figure 3: Schematic diagram of ground truth label categories. (a) Original data (RGB image), (b) Ground truth labels.

2.6.3 Evaluation Index

This study uses overall accuracy (OA), F1-score, and the Kappa coefficient as assessment metrics to evaluate classification accuracy. The formulas for each metric are explained below.

$$OA = \frac{TP+TN}{TP+FP+TN+FN}, \quad (2)$$

$$\text{F1} - \text{score} = \frac{2\times TP}{2\times TP+FP+FN}, \quad (3)$$

$$\text{Kappa} = \frac{P_o - P_e}{1-P_e}, \text{ with} \quad (4)$$

$$P_o = \frac{TP+TN}{TP+FP+TN+FN}, \text{ and} \quad (5)$$

$$P_e = \frac{(TP+FN)\times(TP+FP)+(FP+TN)\times(FN+TN)}{(TP+FP+TN+FN)^2}, \quad (6)$$

Among them, *TP* (true positive), *TN* (true negative), *FP* (false positive), and *FN* (false negative).

3. Results

3.1 Feature Combination Comparison

This study explores four feature combinations using spectral bands, vegetation indices, and texture features for classifying bare land, forest, krummholz, and shadow with the RF and U-Net models. The F1-score results are shown in Fig. 4. Overall, the F1-score exceeds 0.6 for all classes. Since forest and krummholz are both vegetation types, they tend to influence each

https://doi.org/10.5194/egusphere-2025-969
Preprint. Discussion started: 14 April 2025
© Author(s) 2025. CC BY 4.0 License.

other more, whereas the classification accuracy for bare land and shadow is higher, reaching over 0.8. Comparing the RF and U-Net models, the RF model exhibits more stable F1-score differences across the four feature combinations. In contrast, the U-Net model shows more significant variability in F1-scores.

Regarding feature combinations, in the RF model, bare land and shadow achieve the highest classification accuracy with feature combination 1 with F1-scores of 0.905 and 0.866, respectively, while forest and krummholz perform best with feature combination 4 with F1-scores of 0.827 and 0.776 respectively. Similarly, in the U-Net model, the highest classification accuracy for the bare land category is achieved with feature combination 1 with an F1-score of 0.889, while forest, krummholz, and shadow perform best with feature combination 4 with F1-scores of 0.828, 0.886, and 0.869 respectively.

Table 5 presents the accuracy metrics, including Overall Accuracy (OA) and the Kappa coefficient. As the number of features increases, classification accuracy improves. For both the RF and U-Net models, feature combination 4 yields the highest OA values of 0.830 and 0.838, respectively, an improvement of 0.011 and 0.085 compared to feature combination 1, which uses only raw spectral bands. The best Kappa values also correspond to feature combination 4 with scores of 0.768 and 0.778, respectively, showing an increase of 0.015 and 0.112 compared to feature combination 1.

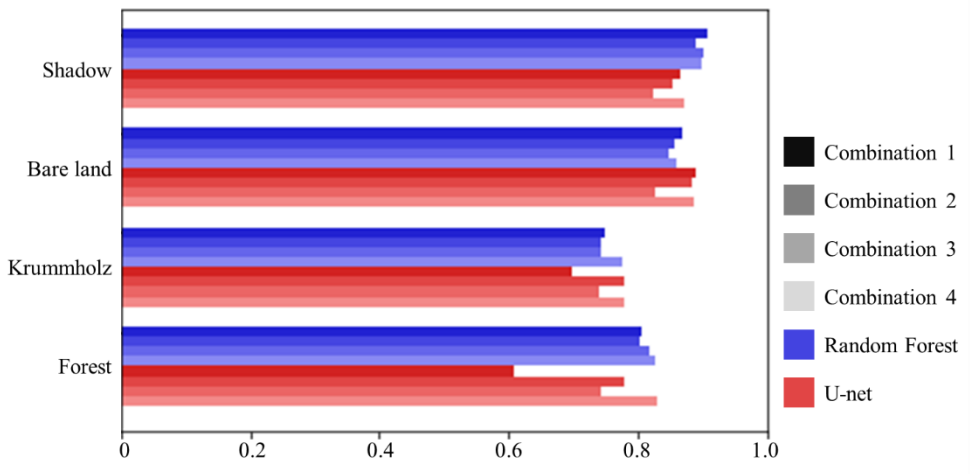

Figure 4: F1-score of Different Categories for RF and U-Net with Various Feature Combinations

Table 5: Evaluation of Classification Accuracy for Different Feature Combinations in RF and U-Net Models

Feature (DIMs)	Combinations 1(8)		Combinations 2(21)		Combinations 3(64)		Combinations 4(77)	
Method	RF	U-Net	RF	U-Net	RF	U-Net	RF	U-Net
OA	0.819	0.753	0.817	0.780	0.812	0.819	0.830	**0.838**
Kappa	0.753	0.666	0.751	0.703	0.743	0.755	0.768	**0.778**

https://doi.org/10.5194/egusphere-2025-969
Preprint. Discussion started: 14 April 2025
© Author(s) 2025. CC BY 4.0 License.

3.2 Feature Importance Selection Based on Random Forest Model

The treeline is determined based on the boundary between bare land, forests, and krummholz. Therefore, after integrating the results from Section 3.1, further analysis was conducted using Feature Combinations 4 and the U-Net model. Since an increase in the number of features leads to longer model training times, it is necessary to evaluate both classification accuracy and computational time costs. To address this, this study utilized the feature importance ranking function of the RF model to rank the importance of the 77 features. The feature ranking results are shown in Fig. 5. Based on cumulative model interpretability, 95% cumulative interpretability can be obtained by 61 features. Further analysis revealed that according to the ranking, the most important features were SEVI, Y, B, G, and NDVI2.

In contrast, texture features were relatively less important. Using these 61 selected features, a retraining process was conducted. The classification results were similar before and after feature selection (Fig. 6), while training time was reduced by 14.3%. Additionally, the overall accuracy (OA) and Kappa coefficient showed a slight improvement of 0.4% compared to the original model (Table 6).

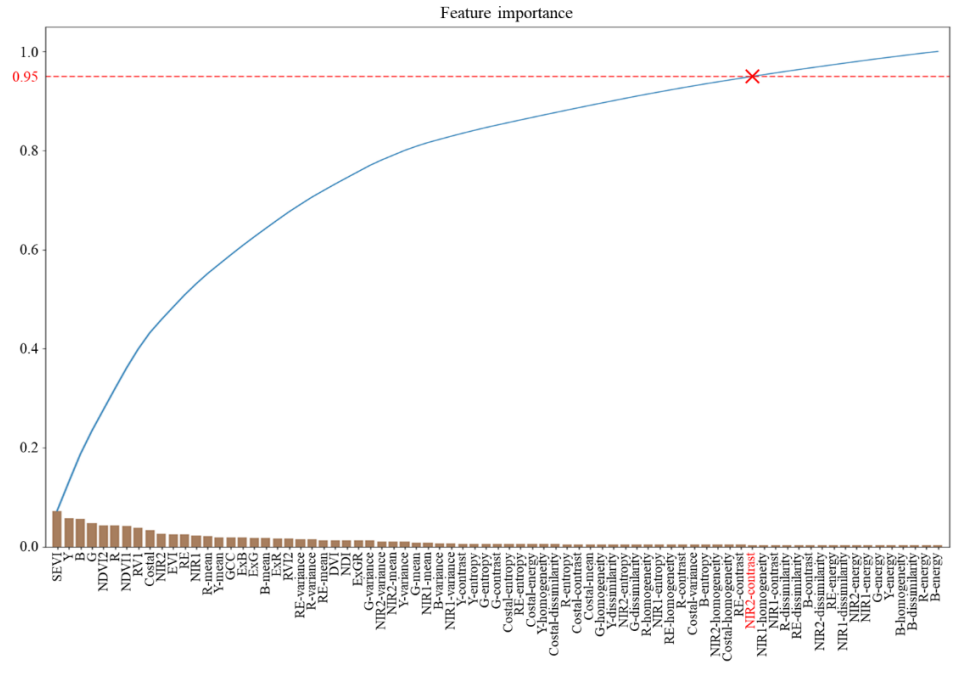

Figure 5: RF model feature importance ranking

Table 6: Comparison of model results with and without feature selection

	Without feature selection	With feature selection	Difference (%)
Training time(s)	27750	23789	-14.3
OA	0.838	0.842	+0.4
Kappa	0.778	0.784	+0.4

https://doi.org/10.5194/egusphere-2025-969
Preprint. Discussion started: 14 April 2025
© Author(s) 2025. CC BY 4.0 License.

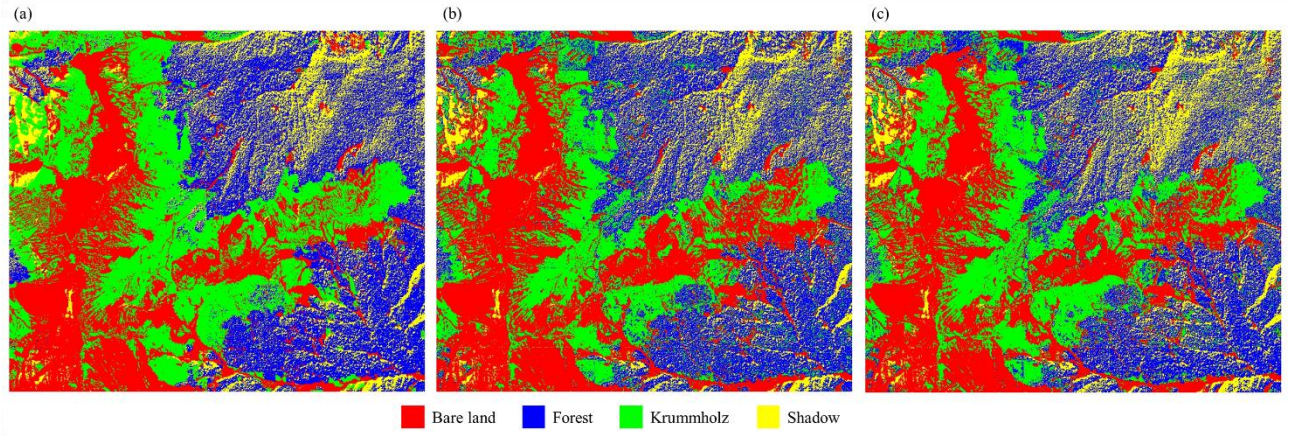

Figure 6: Model classification results with/without feature selection (a) Ground truth (b) Without feature selection (c) With feature selection

3.3 Decade Changes of the treeline

A U-Net model was trained using 61 selected features based on feature importance, and the trained model was then used to classify the images from 2012 and 2021. The classification results from 2012 and 2021 were compared with field survey data, as shown in Fig. 7. The results indicate that the tree line derived from the classification aligns with the tree line edge identified in the field survey. Over a decade, the proportion of forest and shadow areas increased by 3.4% and 8.5%, respectively, while krummholz decreased by 3.2% and bare land decreased by 8.7% (Table 7). For the forest category, changes in forest area showed an expansion of 0.105 km² and a reduction of 0.004 km² between 2012 and 2021 (Fig. 8). The elevation distribution of the forest area shifted from 3,699 m to 3,713 m, reflecting a 14 m rise, as shown in Table 8. The differences in area changes across different elevation ranges are detailed in Table 9, with the most significant changes occurring in the 3,500 to 3,600 m range. In comparison, the most stable area was observed in the 3,700 to 3,800 m range.

https://doi.org/10.5194/egusphere-2025-969
Preprint. Discussion started: 14 April 2025
© Author(s) 2025. CC BY 4.0 License.

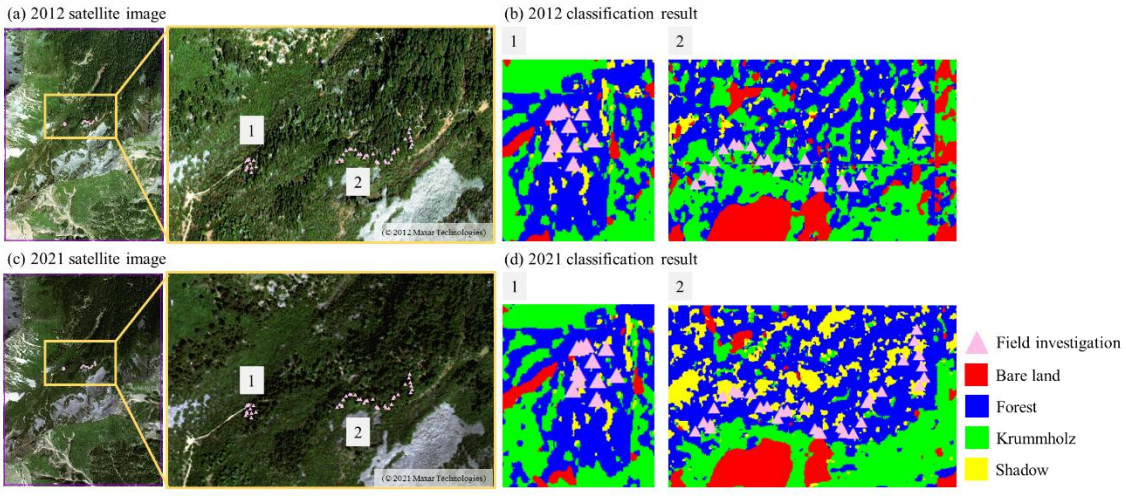

Figure 7 Classified results and spatial distribution of field survey points (a) 2012 Satellite Image (b) 2012 Classified Results (c) 2021 Satellite Image (d) 2021 Classified Results

Table 7: Proportion of classified results from 2012 to 2021

Classification percentage (%)	Year		Increment / Decrement
	2012	2021	
Forest	22.5	25.9	+3.4
Krummholz	36.4	33.2	-3.2
Bare land	38.1	29.4	-8.7
Shadow	3.0	11.5	+8.5
Total	100	100	

https://doi.org/10.5194/egusphere-2025-969
Preprint. Discussion started: 14 April 2025
© Author(s) 2025. CC BY 4.0 License.

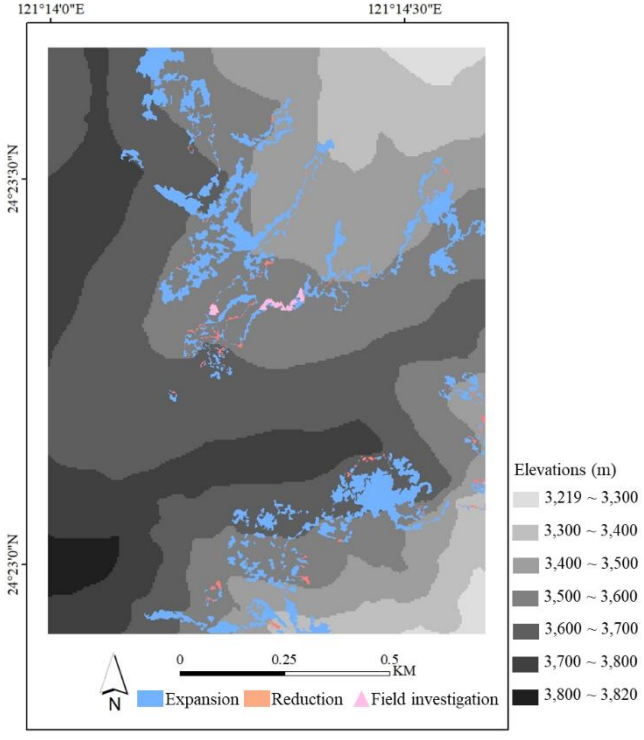

Figure 8: Forest area changes in 2021 and 2012

Table 8: Forest area and highest point height difference from 2012 to 2021

Year	Forest area (km^2)	Elevation (m)
2012	0.463	3,699
2021	0.564	3,713
Difference	+0.101	+14

Table 9: Changes in area differences at different elevations from 2012 to 2021

Elevations (m)	Expansion area (km^2)	Reduction area (km^2)
3300~3400	0.0028	0.0003
3400~3500	0.0221	0.0008
3500~3600	0.0510	0.0023
3600~3700	0.0288	0.0006
3700~3800	0.0002	0.0000

https://doi.org/10.5194/egusphere-2025-969
Preprint. Discussion started: 14 April 2025
© Author(s) 2025. CC BY 4.0 License.

4. Discussion

4.1 Treeline change and spatial pattern

Observing the ecological processes and changes of the alpine treeline (ATE) can help assess the impacts of climate change in different regions. In the Rocky Mountains of Canada, Davis et al. (2020) investigated the changes in four tree species (*Abies lasiocarpa, Larix lyallii, Picea engelmannii, Pinus albicaulis*). They found that overall forest stand density increased, with tree distribution advancing upslope toward the treeline at an average rate of 0.83 ± 0.67 m/year. In the European Alps, researchers observed a significant reduction in snow cover. At the same time, the productivity of alpine treeline vegetation increased, enhancing the ability to sequester atmospheric CO_2 and mitigating the effects of climate change (Rumpf et al., 2022). In the Himalayas of Asia, climate impacts have led to more than 80% of trees in the eastern region reaching the thermal treeline, the potential upper range limit set by the growing season temperature. It is predicted that by the end of the 21st century, trees in the east region will migrate upslope by 140 meters (Wang et al., 2022). Similarly, in Taiwan's Hehuan Mountain and Yushan, studies have also found that alpine treelines are shifting to higher elevations, accompanied by a significant increase in forest density (Greenwood et al., 2014; Chung et al., 2021). This study also found that the alpine treeline's elevation in the Xue Mountain glacial cirque increased by 14 meters between 2012 and 2021, which aligns with the findings of previous studies.

Regarding ATE spatial patterns, Bader et al. (2021) classified alpine treeline patterns into discrete and gradual categories, further distinguishing them into gradual, diffuse, abrupt-diffuse, abrupt, and tree island treelines. Based on the classification results derived from high-resolution satellite imagery, this study identified the treeline patterns in the Xue Mountain glacial cirque as abrupt and tree island treeline patterns. However, additional long-term field observations are required to further investigate the underlying treeline dynamics and demographic processes (Liao et al., unpublished data).

4.2 Feature importance

A total of 77 features were derived from the satellite images, including eight spectral bands, 13 vegetation indices, and 56 texture features. Different features have varying degrees of importance for image classification; therefore, an analysis of feature importance must be conducted based on the classification target. In the alpine treeline (ATE) of Xue Mountain, the primary tree species is Taiwan fir (*Abies kawakamii*), which belongs to coniferous forests. Numerous studies have explored the contribution of satellite image bands to conifer species classification and forest land cover mapping. Several researchers using Sentinel-2 imagery have found that shortwave infrared, red, and near-infrared bands are particularly suitable for identifying land cover and different tree species, with the red band being the most effective for coniferous tree indices (Bolyn et al., 2018; Immitzer et al., 2019; Hościło and Lewandowska, 2019). Using WorldView-2 imagery to study Johannesburg, South Africa, other researchers identified the green, yellow, red, and near-infrared-2 bands as the most critical features for vegetation classification (Abutaleb et al., 2021). Similarly, a study classifying natural forests based on WorldView-2 images in eastern Austria found that the blue, green, red, and near-infrared-1 bands were the most significant (Immitzer et al., 2012). In this

https://doi.org/10.5194/egusphere-2025-969
Preprint. Discussion started: 14 April 2025
© Author(s) 2025. CC BY 4.0 License.

study, the most important bands identified were SEVI, Y, B, G, and NDVI2. Most top-ranked features were spectral bands and vegetation indices, while texture features were less important. Based on these findings, this study concludes that the importance of features varies depending on the region characteristics and classification target.

5. Conclusions

This study investigates the changes in the ATE of the Xue Mountain glacial cirques in Taiwan between 2012 and 2021. Specifically, the study employs the RF and U-Net models to generate classification maps of the ATE and analyse changes in bare land, forest, krummholz, and shadow areas based on WorldView-2 satellite imagery-derived vegetation indices and texture features. The results show that incorporating vegetation indices and texture features alongside the spectral bands improves classification accuracy. The best result is the U-Net model with OA 0.838, which is 0.085 higher than the model using spectral bands alone, and the Kappa coefficient is 0.112 higher. With the selection of feature importance, training time was reduced by 14.3%, with a slight improvement in accuracy. The most significant features were SEVI, Y, B, G, and NDVI2. Comparing the classification results from 2012 and 2021 with field surveys, the treeline edges in the classification maps aligned well with surveyed locations. Over a decade, the spatial coverage of trees increased by approximately 0.101 km², indicating a denser forest situation. Additionally, the elevation of forest distribution is found in higher elevations (rise by 14 meters), representing a gradual upward treeline shift. The most significant changes occurred between 3,500 m and 3,600 m, while the 3,700 m to 3,800 m range remained relatively stable. These findings provide essential scientific insights for future ecosystem management in Xue Mountain and demonstrate the effectiveness of satellite imagery in monitoring alpine treeline ATE dynamics, highlighting its significance for biodiversity conservation and sustainable environmental development.

Data availability

Data are available upon request from the corresponding author (Hui Ping Tsai).

Author contributions

Conceptualization, GGW, MCL, WW, HPT and HYT; methodology, GGW, MCL, WW, HPT and HYT; software, GGW, and HPT; validation, GGW, MCL, WW, HPT and HYT; formal analysis, GGW, HPT and HYT; investigation, GGW, MCL, WW, HPT and HYT; resources, MCL, HPT and HYT; data curation, GGW, MCL and WW; writing—original draft preparation, GGW and HPT; writing—review and editing, MCL, HPT and HYT; visualization, GGW and HPT; supervision, HPT and HYT; project administration, HPT and HYT; funding acquisition, MCL, HPT and HYT. All authors have read and agreed to the published version of the manuscript.

https://doi.org/10.5194/egusphere-2025-969
Preprint. Discussion started: 14 April 2025
© Author(s) 2025. CC BY 4.0 License.

Competing interests

The authors declare that they have no conflict of interest.

Acknowledgments

This work was partially financially supported by the "Innovation and Development Center of Sustainable Agriculture" from The Featured Areas Research Center Program within the framework of the Higher Education Sprout Project by the Ministry of Education (MOE) in Taiwan. Additionally, the support also provided by the National Science and Technology Council under projects 111-2313-B-054-001, 112-2321-B-005-007-, 112-2634-F-005-002-, 112-2119-M-005-001-, 112-2121-M-005-003-, 113-2321-B-005-005-, 113-2634-F-005-002-, 113-2119-M-005-001-, 113-2121-M-005-005- and Shei-Pa National Park Headquarters, National Park Service, Ministry of the Interior under project SP113110.

References

Abutaleb, K., Newete, S. W., Mangwanya, S., Adam, E., and Byrne, M. J.: Mapping eucalypts trees using high resolution multispectral images: A study comparing WorldView 2 vs. SPOT 7. Egypt. J. Remote Sens. Space Sci., 24(3), 333-342, https://doi.org/10.1016/j.ejrs.2020.09.001, 2021.

Bader, M. Y., Llambí, L. D., Case, B. S., Buckley, H. L., Toivonen, J. M., Camarero, J. J., Cairns, D. M., Brown, C. D., Wiegand, T., and Resler, L. M.: A global framework for linking alpine-treeline ecotone patterns to underlying processes. Ecography, 44(2), 265-292, https://doi.org/10.1111/ecog.05285, 2021.

Belgiu, M., and Drăguț, L.: Random forest in remote sensing: A review of applications and future directions. ISPRS J. Photogramm. Remote Sens. 114, 24-31, https://doi.org/10.1016/j.isprsjprs.2016.01.011, 2016.

Bolyn, C., Michez, A., Gaucher, P., Lejeune, P., and Bonnet, S.: Forest mapping and species composition using supervised per pixel classification of Sentinel-2 imagery. Biotechnol. Agron. Soc., 22(3), https://doi.org/10.25518/1780-4507.16524, 2018.

Boutaba, R., Salahuddin, M. A., Limam, N., Ayoubi, S., Shahriar, N., Estrada-Solano, F., and Caicedo, O. M.: A comprehensive survey on machine learning for networking: evolution, applications and research opportunities. J. Internet Serv. Appl., 9(1), 1-99, https://doi.org/10.1186/s13174-018-0087-2, 2018.

Breiman, L.: Random forests. Mach. Learn., 45, 5-32, https://doi.org/10.1023/A:1010933404324, 2001.

Chen, J., Tan, R., and Yang, Y.: Research on an innovative feature importance recognition algorithm based on GINI-OOB index, in 2023 IEEE International Conference on Image Processing and Computer Applications (ICIPCA), Changchun, China, 862-866, https://doi.org/10.1109/ICIPCA59209.2023.10257830, 2023.

https://doi.org/10.5194/egusphere-2025-969
Preprint. Discussion started: 14 April 2025
© Author(s) 2025. CC BY 4.0 License.

Chen, W., Ding, H., Li, J., Chen, K., and Wang, H.: Alpine treelines as ecological indicators of global climate change: Who has studied? What has been studied?. Ecol. Inform., 70, 101691, https://doi.org/10.1016/j.ecoinf.2022.101691, 2022

Chiu, C. A., Tzeng, H. Y., Lin, C. T., Chang, K. C., and Liao, M. C.: Spatial distribution and climate warming impact on *Abies kawakamii* forest on a subtropical island. Plants, 11(10), 1346, https://doi: 10.3390/plants11101346, 2022.

Chung, M. E., Doyog, N. D., and Lin, C.: Monitoring of the trend of timberlines in Taiwan amidst climate change through multi-temporal satellite images, in 2021 IEEE International Geoscience and Remote Sensing Symposium IGARSS, Brussels, Belgium, 6488-6491, https://doi.org/10.1109/IGARSS47720.2021.9553538, 2021.

Davis, E. L., Brown, R., Daniels, L., Kavanagh, T., and Gedalof, Z. E.: Regional variability in the response of alpine treelines to climate change. Clim. Change, 162(3), 1365-1384, https://doi.org/10.1007/s10584-020-02743-0, 2020.

Du, H., Liu, J., Li, M. H., Büntgen, U., Yang, Y., Wang, L., Wu, Z., and He, H. S.: Warming-induced upward migration of the alpine treeline in the Changbai Mountains, northeast China. Global Change Biol., 24(3), 1256-1266, https://doi.org/10.1111/gcb.13963, 2018.

Engler, R., Randin, C. F., Thuiller, W., Dullinger, S., Zimmermann, N. E., Araújo, M. B., Pearman, P. B., Lay, G. L., Piedallu, C., Albert, C. H., Choler, P., Coldea, G., Lamo, X. D., Dirnböck, T., Gégout, J. C., Gómez-García, D., Grytnes, J. A., Heegaard, E., Høistad, F., Nogués-Bravo, D., Normand, S., Puşcaş, M., Sebastià, M. T., Stanisci, A., Theurillat, J. P., Trivedi, M. R., Vittoz, P., and Guisan, A.: 21st century climate change threatens mountain flora unequally across Europe. Global Change Biol., 17(7), 2330-2341, https://doi.org/10.1111/j.1365-2486.2010.02393.x, 2011.

Freudenberg, M., Nölke, N., Agostini, A., Urban, K., Wörgötter, F., and Kleinn, C.: Large scale palm tree detection in high resolution satellite images using U-Net. Remote Sens., 11(3), 312, https://doi.org/10.3390/rs11030312, 2019.

Gillespie, A. R., Kahle, A. B., and Walker, R. E.: Color enhancement of highly correlated images. II. Channel ratio and "chromaticity" transformation techniques. Remote Sens. Environ., 22(3), 343-365, https://doi.org/10.1016/0034-4257(87)90088-5, 1987.

Gitelson, A., and Merzlyak, M. N.: Spectral reflectance changes associated with autumn senescence of *Aesculus hippocastanum* L. and *Acer platanoides* L. leaves. Spectral features and relation to chlorophyll estimation. J. Plant Physiol., 143(3), 286-292, https://doi.org/10.1016/S0176-1617(11)81633-0, 1994.

Greenwood, S., Chen, J. C., Chen, C. T., and Jump, A. S.: Strong topographic sheltering effects lead to spatially complex treeline advance and increased forest density in a subtropical mountain region. Glob. Change Biol., 20(12), 3756-3766, https://doi.org/10.1111/gcb.12710, 2014.

Guo, W., Rees, G., and Hofgaard, A.: Delineation of the forest-tundra ecotone using texture-based classification of satellite imagery. Int. J. Remote Sens., 41(16), 6384-6408, https://doi.org/10.1080/01431161.2020.1734254, 2020.

Hall-Beyer, M.: GLCM Texture: A Tutorial v. 3.0 March 2017, 2017.

Hościło, A., and Lewandowska, A. Mapping forest type and tree species on a regional scale using multi-temporal Sentinel-2 data. Remote Sens., 11(8), 929, https://doi.org/10.3390/rs11080929, 2019.

Hsu, S. Y.: Texture-tone analysis for automated land-use mapping. Photogramm. Eng. Remote Sens., 44(11), 1393-1404, 1978.

https://doi.org/10.5194/egusphere-2025-969
Preprint. Discussion started: 14 April 2025
© Author(s) 2025. CC BY 4.0 License.

Huete, A., Didan, K., Miura, T., Rodriguez, E. P., Gao, X., and Ferreira, L. G.: Overview of the radiometric and biophysical performance of the MODIS vegetation indices. Remote Sens. Environ., 83(1-2), 195-213, https://doi.org/10.1016/S0034-4257(02)00096-2, 2002

Huss, M., Bookhagen, B., Huggel, C., Jacobsen, D., Bradley, R. S., Clague, J. J., Vuille, M., Buytaert, W., Cayan, D. R., Greenwood, G., Mark, B. G., Milner, A. M., Weigartner, R., and Winder, M.: Toward mountains without permanent snow and ice. Earth's Future, 5, 418-435, https://doi.org/10.1002/2016EF000514, 2017.

Immitzer, M., Atzberger, C., and Koukal, T.: Tree species classification with random forest using very high spatial resolution 8-band WorldView-2 satellite data. Remote Sens., 4(9), 2661-2693, https://doi.org/10.3390/rs4092661, 2012.

Immitzer, M., Neuwirth, M., Böck, S., Brenner, H., Vuolo, F., and Atzberger, C.: Optimal input features for tree species classification in Central Europe based on multi-temporal Sentinel-2 data. Remote Sens., 11(22), 2599, https://doi.org/10.3390/rs11222599, 2019.

Jackson, C. M., and Adam, E.: Machine learning classification of endangered tree species in a tropical submontane forest using worldview-2 multispectral satellite imagery and imbalanced dataset. Remote Sens., 13(24), 4970, https://doi.org/10.3390/rs13244970, 2021.

Jiang, H., Wang, S., Cao, X., Yang, C., Zhang, Z., and Wang, X.: A shadow-eliminated vegetation index (SEVI) for removal of self and cast shadow effects on vegetation in rugged terrains. Int. J. Digit. Earth, 12(9), 1013-1029, https://doi.org/10.1080/17538947.2018.1495770, 2019.

Johnson, J. S., Gaddis, K. D., Cairns, D. M., and Krutovsky, K. V.: Seed dispersal at alpine treeline: An assessment of seed movement within the alpine treeline ecotone. Ecosphere, 8(1), e01649, https://doi.org/10.1002/ecs2.1649, 2017.

Jombo, S., Adam, E., Byrne, M. J., and Newete, S. W.: Evaluating the capability of Worldview-2 imagery for mapping alien tree species in a heterogeneous urban environment. Cogent Soc. Sci., 6(1), 1754146, https://doi.org/10.1080/23311886.2020.1754146, 2020.

Jordan, C. F.: Derivation of leaf-area index from quality of light on the forest floor. Ecol., 50(4), 663-666, https://doi.org/10.2307/1936256, 1969

Körner, C.: Treelines will be understood once the functional difference between a tree and a shrub is. Ambio, 41(Suppl 3), 197-206, https://doi.org/10.1007/s13280-012-0313-2, 2012.

Kuo, C. C., Liu, Y. C., Su, Y., Liu, H. Y., and Lin, C. T.: Responses of alpine summit vegetation under climate change in the transition zone between subtropical and tropical humid environment. Sci. Rep., 12(1), 13352, https://doi.org/10.1038/s41598-022-17682-2,2022.

Larrinaga, A. R., and Brotons, L.: Greenness indices from a low-cost UAV imagery as tools for monitoring post-fire forest recovery. Drones, 3(1), 6, https://doi.org/10.3390/drones3010006, 2019

Li, M. H., Jiang, Y., Wang, A., Li, X., Zhu, W., Yan, C. F., Du, D., Shi, Z., Lei, J., Schönbeck, L., He, P., Yu, F. H., and Wang, X.: Active summer carbon storage for winter persistence in trees at the cold alpine treeline. Tree Physiolo., 38(9), 1345-1355, https://doi.org/10.1093/treephys/tpy020, 2018.

https://doi.org/10.5194/egusphere-2025-969
Preprint. Discussion started: 14 April 2025
© Author(s) 2025. CC BY 4.0 License.

Li, P. H., Liao, M. C., Tzeng, H. Y., Tseng, Y. H., and Yen, T. M.: Applicability evaluation of tree volume equation for *Abies kawakamii* (Hayata) Ito based on stem analysis data in Taiwan. J. For. Res., 26(5), 336-343, https://doi.org/10.1080/13416979.2021.1927502, 2021.

Liao, M. C. Wang, W., and Tzeng H. Y.: Study of the Structure and Competitive Coexistence of Subalpine Krummholz Species in Taiwan. Taiwan J. For. Sci., 38(3), 203-220, https://doi.org/10.7075/TJFS.202309_38(3).0002, 2023a.

Liao, M. C., Li, P. H., Wang, W., Chiu, C. A., and Tzeng, H. Y.: Structure changes of the subalpine Taiwan fir (*Abies kawakamii* (Hay.) Ito) forest from 2008 to 2018. J. For. Res., 28(2), 126-135, https://doi.org/10.1080/13416979.2022.2135523, 2023b.

Lin, J. C., Chiou, C. R., Chan, W. H., and Wu, M. S.: Valuation of forest ecosystem services in Taiwan. Forests, 12(12), 1694, https://doi.org/10.3390/f12121694, 2021.

Loranger, H., Zotz, G., and Bader, M. Y.: Early establishment of trees at the alpine treeline: Idiosyncratic species responses to temperature-moisture interactions. AoB Plants, 8, plw053, https://doi.org/10.1093/aobpla/plw053, 2016.

Mao, W., Wang, Y., and Wang, Y.: Real-time detection of between-row weeds using machine vision. In: 2003 ASAE Annual Meeting (p. 1). American Society of Agricultural and Biological Engineers, https://doi.org/10.13031/2013.15381, 2003

Materka, A., and Strzelecki, M.: Texture analysis methods–a review. Technical University of Lodz, Institute of Electronics, COST B11 Report, Brussels, 9–11, 1998

Meyer, G. E., and Neto, J. C.: Verification of color vegetation indices for automated crop imaging applications. Comput. Electron. Agric., 63(2), 282-293, https://doi.org/10.1016/j.compag.2008.03.009, 2008.

Meyer, G. E., Hindman, T. W., and Laksmi, K.: Machine vision detection parameters for plant species identification. In: Precision agriculture and biological quality, 14, January, 1999, 3543, 327-335, https://doi.org/10.1117/12.336896, 1999

Mohapatra, J., Singh, C. P., Tripathi, O. P., and Pandya, H. A.: Remote sensing of alpine treeline ecotone dynamics and phenology in Arunachal Pradesh Himalaya. Int. J. Remote Sens., 40(20), 7986-8009, https://doi.org/10.1080/01431161.2019.1608383, 2019.

Richardson, A. J., and Wiegand, C. L.: Distinguishing vegetation from soil background information. Photogramm. Eng. Remote Sens., 43(12), 1541-1552, 1977.

Ronneberger, O., Fischer, P., and Brox, T.: U-net: Convolutional networks for biomedical image segmentation, in: Medical image computing and computer-assisted intervention–MICCAI 2015: 18th international conference, Munich, Germany, 5-9, October, 2015, proceedings, part III 18. Springer international publishing, edited by: Navab, N., Hornegger, J., Wells, W., Frangi, A., Springer, Cham, 234-241, https://doi.org/10.1007/978-3-319-24574-4_28, 2015.

Rösch, M., Sonnenschein, R., Buchelt, S., and Ullmann, T.: Comparing PlanetScope and Sentinel-2 imagery for mapping mountain pines in the Sarntal Alps, Italy. Remote Sens., 14(13), 3190, https://doi.org/10.3390/rs14133190, 2022.

Rouse Jr, J. W., Haas, R. H., Schell, J. A., and Deering, D. W.: Monitoring vegetation systems in the Great Plains with ERTS, in Proceedings of the 3rd ERTS Symposium, Washington, DC, USA, 1, 309-317, 1974

https://doi.org/10.5194/egusphere-2025-969
Preprint. Discussion started: 14 April 2025
© Author(s) 2025. CC BY 4.0 License.

Rubner, Y., Puzicha, J., Tomasi, C., and Buhmann, J. M.: Empirical evaluation of dissimilarity measures for color and texture. Comput. Vis. Image Underst., 84(1), 25-43, https://doi.org/10.1006/cviu.2001.0934, 2001.

Rumpf, S. B., Gravey, M., Brönnimann, O., Luoto, M., Cianfrani, C., Mariethoz, G., and Guisan, A.: From white to green: Snow cover loss and increased vegetation productivity in the European Alps. Science, 376(6597), 1119-1122, https://doi.org/10.1126/science.abn6697, 2022.

Sibiya, B., Lottering, R., and Odindi, J.: Discriminating commercial forest species using image texture computed from a worldview-2 pan-sharpened image and partial least squares discriminant analysis. Remote Sens. Appl.: Soc. Environ., 23, 100605, https://doi.org/10.1016/j.rsase.2021.100605, 2021.

Sonnentag, O., Hufkens, K., Teshera-Sterne, C., Young, A. M., Friedl, M., Braswell, B. H., Milliman, T., O'Keefe, J., and Richardson, A. D.: Digital repeat photography for phenological research in forest ecosystems. Agric. For. Meteorol., 152, 159-177, https://doi.org/10.1016/j.agrformet.2011.09.009, 2012.

Terskaia, A., Dial, R. J., and Sullivan, P. F.: Pathways of tundra encroachment by trees and tall shrubs in the western Brooks Range of Alaska. Ecography, 43(5), 769-778, https://doi.org/10.1111/ecog.05015, 2020.

Wagner, F. H., Sanchez, A., Tarabalka, Y., Lotte, R. G., Ferreira, M. P., Aidar, M. P. M., Gloor, E., Phillips, O. L., and Aragão, L. E. O. C.: Using the U-net convolutional network to map forest types and disturbance in the Atlantic rainforest with very high resolution images. Remote Sens. Ecol. Conserv., 5(4), 360-375, https://doi.org/10.1002/rse2.111, 2019.

Wang, H., Zhao, Y., Pu, R., and Zhang, Z.: Mapping *Robinia pseudoacacia* forest health conditions by using combined spectral, spatial, and textural information extracted from IKONOS imagery and random forest classifier. Remote Sens., 7(7), 9020-9044, https://doi.org/10.3390/rs70709020, 2015.

Wang, W., Liao, M. C., and Tzeng, H. Y.: Competition in *Abies kawakamii* forests at subtropical high mountain in Taiwan. PLoS ONE, 16(7), e0254791, https://doi.org/10.1371/journal.pone.0254791, 2021.

Wang, X., Wang, T., Xu, J., Shen, Z., Yang, Y., Chen, A., Wang, S., Liang, E., and Piao, S.: Enhanced habitat loss of the Himalayan endemic flora driven by warming-forced upslope tree expansion. Nat. Ecol. Evol., 6(7), 890-899, https://doi.org/10.1038/s41559-022-01774-3, 2022.

Wang, Y., Pederson, N., Ellison, A. M., Buckley, H. L., Case, B. S., Liang, E., and Julio Camarero, J.: Increased stem density and competition may diminish the positive effects of warming at alpine treeline. Ecol., 97(7), 1668-1679, https://doi.org/10.1890/15-1264.1, 2016.

Woebbecke, D. M., Meyer, G. E., Von Bargen, K., and Mortensen, D. A.: Color indices for weed identification under various soil, residue, and lighting conditions. Transactions of the ASAE, 38(1), 259-269, https://doi.org/10.13031/2013.27838, 1995

Xu, D., Geng, Q., Jin, C., Xu, Z., and Xu, X.: Tree line identification and dynamics under climate change in Wuyishan National Park based on Landsat images. Remote Sens., 12(18), 2890, https://doi.org/10.3390/rs12182890, 2020.

Yuan, X., King, D., and Vlcek, J.: Sugar maple decline assessment based on spectral and textural analysis of multispectral aerial videography. Remote Sens. Environ., 37(1), 47-54, https://doi.org/10.1016/0034-4257(91)90049-C, 1991.

https://doi.org/10.5194/egusphere-2025-969
Preprint. Discussion started: 14 April 2025
© Author(s) 2025. CC BY 4.0 License.

Zheng, Z., Zhu, W., and Zhang, Y.: Seasonally and spatially varied controls of climatic factors on net primary productivity in alpine grasslands on the Tibetan Plateau. Glob. Ecol. Conserv., 21, e00814, https://doi.org/10.1016/j.gecco.2019.e00814, 2020.

480